

# INF574: Digital Representations and Analysis of Shapes

## Shape Comparison and Retrieval

Pegah Khayatan, Veronika Shilova

### Contents

<b>1</b>	<b>Introduction</b>	<b>1</b>
<b>2</b>	<b>Retrospective of shape retrieval methods: from first descriptors to state-of-the-art models</b>	<b>2</b>
<b>3</b>	<b>Theoretical aspects</b>	<b>3</b>
3.1	Laplace-Beltrami operator . . . . .	3
3.2	Shape DNA . . . . .	4
3.3	Global Point Signature . . . . .	4
<b>4</b>	<b>Classification</b>	<b>5</b>
4.1	G2-distribution . . . . .	5
4.2	Dataset . . . . .	5
<b>5</b>	<b>Results and Analysis</b>	<b>6</b>
<b>6</b>	<b>Conclusion</b>	<b>6</b>
<b>7</b>	<b>Appendix</b>	<b>8</b>
<b>8</b>	<b>Definitions</b>	<b>10</b>

### 1 Introduction

The characterization of 3D objects is of great importance in the field of computer graphics and geometric modeling and basic questions such as quickly identifying and retrieving an object from a huge dataset has been a long standing problem; the latter is called shape retrieval. To find such a characterization, different methods have been introduced before using the eigenvalues of the Laplace-Beltrami operator, usually based on one of the following approaches: realigning an object or decomposing an object into smaller features which would be compared in a second step. However, these methods were restrictive and not robust to certain deformations. Moreover, these methods depended largely on the type of the representation that is used for shapes; even when restricted to one type of boundary representation such as non-uniform rational basis spline, it is not easy to decide if the given objects are similar in their shape. A simple comparison of the control points used to represent the boundary surfaces does not help at all, because identical patches can be represented with different control points. To overcome these restrictions new methods have been

introduced that use eigenvalues and eigenvectors of the Laplace–Beltrami operator as embeddings for isometric shapes. These methods were introduced relatively much later than other works in the field; a major reason behind this lag has been the lack of computationally powerful hardware to calculate spectra of the Laplace–Beltrami operator.

The goal of this project is to compare two kind of shape descriptors based on Laplace–Beltrami operator: one that uses its eigenvalues directly [Reuter et al. \[2006\]](#) and the other which derives a deformation invariant representation of surfaces from its eigenvalues and eigenfunctions, namely the GPS embedding. The difference between these two methods, as mentioned in [Rustamov \[2007\]](#), is that the shape DNA which is the set of Laplace–Beltrami eigenvalues – the spectrum – does not determine the surface uniquely up to isometry; there are so called isospectral shapes – non-isometric surfaces that have coinciding spectra. This flaw is overcome in the latter work.

In the following report we first explain the fundamentals of the Shape DNA technique for shape retrieval and then we further explore the different approach used in [Rustamov \[2007\]](#). We will then have a closer look over the efficiency of each method tested on the [Sumner and Popovic \[2013\]](#) dataset.

## 2 Retrospective of shape retrieval methods: from first descriptors to state-of-the-art models

Isometry invariants are very often used to characterize a 3D object; these isometry invariants are desirable for this task as they only depend on the intrinsic shape and also are independent of the embedding and the spatial position. One such method can use topological invariants such as homology groups and Betti numbers; however, they are unable to distinguish homeomorphic shapes [Seifert and Threlfall \[1980\]](#).

The first fundamental tensor (defined independently of a parametrization) is a complete isometry invariant. However, this invariant can generally not be used to check if two given parametrizations represent isometric manifolds. Parametrizing to a common representation is needed before comparing this invariant for two objects [Do Carmo \[1976\]](#).

Another complete shape descriptor is the medial axis transform (MAT). Using the MAT for testing the [congruence](#) of two given 3d-solids would also require checking if the respective medial axis sets (usually collections of surface patches) are congruent, a task that again is not easy at all in general. Therefore, none of the shape invariants listed above can be used efficiently to detect if two distinct geometrical object representations refer to congruent or isometric objects.

Nowadays, due to the tremendous success of convolutional neural networks (CNNs) in computer vision, a lot of the state-of-the-art techniques for shape retrieval are based on the generalization of CNNs for shapes. The key ingredient of these methods is defining appropriate notions of convolution and pooling. However, unlike the Euclidean case, there is no universal canonical notion of convolution on surfaces. Existing approaches try to address this problem through a number of solutions such as local parametrizations [Wiersma et al. \[2020\]](#) or applying convolution on the edges of the mesh [Hanocka et al. \[2019\]](#).

There also a number of learning techniques for shapes which are based on diffusion. These approaches learn parameters of the diffusion process that are directly transferable across shapes and can be used effectively in applications like non-rigid shape matching [Hansen et al. \[2018\]](#), [Sharp et al. \[2020\]](#).

### 3 Theoretical aspects

#### 3.1 Laplace-Beltrami operator

For a closed compact manifold surface  $S$ , let  $\Delta$  denote its Laplace-Beltrami differential operator. Consider the equation

$$\Delta\phi = \lambda\phi. \quad (1)$$

A scalar  $\lambda$  for which the equation has a nontrivial solution is called an eigenvalue of  $\Delta$ ; the solution  $\phi$  is called an eigenfunction corresponding to  $\lambda$ . Note that  $\lambda = 0$  is always an eigenvalue – the corresponding eigenfunctions are constant functions.

The eigenvalues of the Laplace-Beltrami operator are non-negative and constitute a discrete set. We will assume that the eigenvalues are distinct, so we can put them into ascending order

$$\lambda_0 = 0 < \lambda_1 < \lambda_2 < \dots < \lambda_i < \dots \quad (2)$$

The appropriately normalized eigenfunction corresponding to  $\lambda_i$  will be denoted by  $\phi_i$ .

The Laplace-Beltrami operator is Hermitian, hence, the eigenfunctions corresponding to its different eigenvalues are orthogonal:

$$\langle \phi_i, \phi_j \rangle = \int_S \phi_i \phi_j = 0. \quad (3)$$

Thus, eigenfunctions of the continuous Laplace-Beltrami operator give an orthogonal basis for the space of functions defined on the surface. Moreover, it is important to note that Laplace-Beltrami operator is isometry invariant.

In discrete setting, the Laplace-Beltrami differential operator can be defined by the discrete Laplacian matrix  $L$  as follows

$$L = \begin{cases} \sum_k \frac{m_{ik}}{s_i}, & \text{if } i = j, \\ -\frac{m_{ij}}{s_i}, & \text{if } i \text{ and } j \text{ are adjacent,} \\ 0, & \text{otherwise,} \end{cases} \quad (4)$$

where  $m_{ij} = \frac{\cot\alpha_{i,j} + \cot\beta_{ij}}{2}$  (the angles appearing in this formula are depicted in the figure 1),  $s_i$  is the area of the shaded region in the figure 1.

The areas  $s_i$  associated with mesh vertices can vary from vertex to vertex, for this reason the discrete Laplacian matrix  $L$  is not symmetric. Finding the discrete counterpart of Laplace-Beltrami eigenvalues and eigenfunctions is equivalent to the standard eigenvalue problem for the matrix  $L$

$$L\phi = \lambda\phi. \quad (5)$$

Since  $L$  is not symmetric, we have no guarantee that the eigenvalues and eigenvectors of  $L$  will be real; even if they were real, the numerical procedures would sometimes yield complex results. Furthermore, it is not clear how to normalize the eigenvectors. Indeed, the eigenfunctions of the continuous Laplace-Beltrami operator are orthogonal, while the eigenvectors of the discrete version are not (if one uses the usual dot product) [Vallet and Lévy [2008]].

To solve these problems, instead of solving system 5, we rewrite it in the following way

$$M\phi = \lambda S\phi, \quad (6)$$

where  $M$  is the matrix

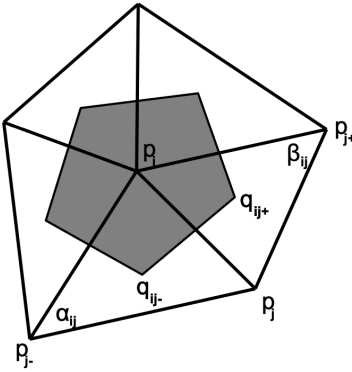


Figure 1: Definitions of the angles and the area appearing in the discrete Laplace-Beltrami operator.

$$M = \begin{cases} \sum_k m_{ik}, & \text{if } i = j, \\ -m_{ij}, & \text{if } i \text{ and } j \text{ are adjacent,} \\ 0, & \text{otherwise,} \end{cases} \quad (7)$$

and  $S$  is diagonal matrix  $S$  with entries  $S_{ii} = s_i$ , and

$$L = S^{-1} M. \quad (8)$$

Although this formulation is equivalent to the standard one, we would get the same real eigenvalues and eigenvectors as in the standard case. The problem 8 is called generalized eigenvalue problem. It is used in our project to compute eigenvalues and eigenfunctions of the discrete Laplacian matrix. To compute the matrices  $M$  and  $S$ , we use the formulas from the paper [Bronstein et al. \[2017\]](#).

### 3.2 Shape DNA

The shape DNA method is based on using the eigenvalues of the Laplace-Beltrami operator as a "fingerprint". It is one of the first spectral shape descriptors. It is defined as the normalized beginning sequence of the eigenvalues of the Laplace-Beltrami operator.

Its main advantages are the simple representation (a vector of numbers) and comparison, scale invariance, and in spite of its simplicity a very good performance for shape retrieval of non-rigid shapes. In the [section 7 Appendix](#) we briefly discuss a number of facts to illustrate certain properties of these eigenvalues.

### 3.3 Global Point Signature

Another approach to obtain a shape representation that is invariant under natural deformations is called Global Point Signature (GPS) embeddings, which is based on combining the Laplace-Beltrami eigenvalues and eigenfunctions.

Let us remind that the Laplace-Beltrami operator and its eigenfunctions are intrinsic in that sense: the values of eigenfunctions can be thought as numbers attached to the points on the surface, these numbers do not depend on how the surface is located in Cartesian coordinates. Thus, it is natural to try to characterize the points by the values of the eigenfunctions.

Given a point  $\mathbf{p}$  on the surface, we define its Global Point Signature,  $GPS(\mathbf{p})$ , as the infinite-dimensional vector

$$GPS(\mathbf{p}) = \left( \frac{1}{\sqrt{\lambda_1}} \phi_1(\mathbf{p}), \frac{1}{\sqrt{\lambda_2}} \phi_2(\mathbf{p}), \frac{1}{\sqrt{\lambda_3}} \phi_3(\mathbf{p}), \dots \right), \quad (9)$$

where where  $\phi_i(\mathbf{p})$  is the value of the eigenfunction  $\phi_i$  at the point  $\mathbf{p}$ .

$GPS$  can be further considered as a mapping of the surface into infinite dimensional space. The image of this map is called the  $GPS$  embedding of the surface.

It is important to note that

1.  $GPS$  embedding is an isometry invariant. This means that two isometric surfaces will have the same image under the  $GPS$  mapping.
2. Given the  $GPS$  embedding and the eigenvalues, one can recover the surface up to isometry.
3. The  $GPS$  embedding is not subject to rotations or translations of the ambient infinite-dimensional space.

From this we conclude that at least theoretically the  $GPS$  embedding provides an ideal tool for processing of non-rigid shapes – matching, segmentation, and correspondence.

## 4 Classification

Our task was to compare Shape DNA and  $GPS$  embeddings approaches on classification task.

### 4.1 G2-distribution

The  $GPS$  embedding gives a deformation independent embedding of a shape into the infinite dimensional space. To achieve fast comparison of shapes, from this embedding we extract a concise descriptor. We do not work with infinite dimensional space, but consider the projection onto the first  $d$  dimensions.

As descriptor we will use  $G2$ -distribution which is built in the following way. After computing  $GPS$  embeddings for each point on the surface, we subdivide the image of the  $GPS$  embedding by  $m$ ,  $m \in \mathbb{N}$ , equally spaced spheres  $S_i$ ,  $i = 1, \dots, m$ , centered at the origin of this  $d$ -dimensional space. We denote  $S_0 = \emptyset$ ,  $R_i = S_i \setminus S_{i-1}$ ,  $i = 1, \dots, m$ , and  $R_{m+1} = \mathbb{R}^d \setminus S_m$ . Then we construct  $m^2$  histograms, each of these histograms captures the distribution of distances between points, one of which belongs to  $R_i$ , the other to  $R_j$ ,  $i, j = 1, \dots, m + 1$ ,  $i \neq j$ .

To compare shapes, we compute the sum of  $L_2$  distances between respective histograms of these shapes.

### 4.2 Dataset

We compare two methods on the [Sumner and Popovic \[2013\]](#) dataset. It has 72 shapes and 8 classes: cat, lion, horse, camel, elephant, flamingo, head and face. Each class has 9 instances in different poses, some examples of possible shapes are shown in figure 2.

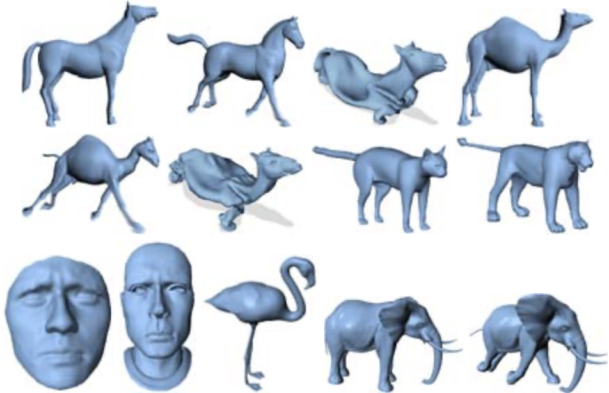


Figure 2: Examples of shapes from the dataset [Sumner and Popovic \[2013\]](#).

## 5 Results and Analysis

Figures 3 and 4 show distance matrices built using distances between the vectors of eigenvalues (we took 10 eigenvalues) for Shape DNA and using the sum of  $L_2$  distances between respective histograms for GPS embedding method. Vivid blue colors on the figures mean that instances are further apart while pale blue colors indicate the opposite. The classes of objects come in groups of 9, so there are 8 contiguous sets of 9 rows, each corresponding to a shape class (e.g., cat, lion, horse, camel). We hope to see a 9x9 pale blue or even white square for each group along the diagonal, with more vivid colors everywhere else in the same row. This means that a particular group is close to itself and far from others when the histogram signatures are compared.

We see that for each plot there is a clear structure in which pale blue squares appear along the diagonal. However, in the case of the Shape DNA descriptor, some squares outside the main diagonal are almost as pale as the diagonal ones in the same row. That means that the shape classes cannot be efficiently separated using Shape DNA descriptor even on a small dataset. As for GPS embeddings, the separation between classes is more clear, we observe that they are further apart according to the distance matrix.

Moreover, from figure 5 we see that classification using GPS embeddings performs accurately enough. As Multidimensional scaling (MDS) shows the level of similarity of instances in a dataset, we conclude that when using GPS embeddings and  $G_2$ -distributions, shape classes are better separated from each other and that  $G_2$ -distributions can distinguish objects belonging to different categories well. It states also that isometric deformations influence the  $G_2$ -distributions only slightly. All of the shapes of different classes are clustered together tightly.

## 6 Conclusion

In this project we studied two shape descriptors which are Shape DNA and  $G_2$ -distribution based on GPS embeddings. Both this approaches are proven to be quite efficient on the classification task. However,  $G_2$ -distribution based method outperformed Shape DNA in classification on [Sumner and Popovic \[2013\]](#) dataset. In this case, GPS embeddings based method is more robust to inner class shape variations and also separates better different classes of shapes. It is also isometry invariant which is important for various problems in shape analysis.

Although GPS embeddings method is quite efficient on our small dataset, it might be not as efficient and robust on large datasets. Moreover, this method is computationally expensive which

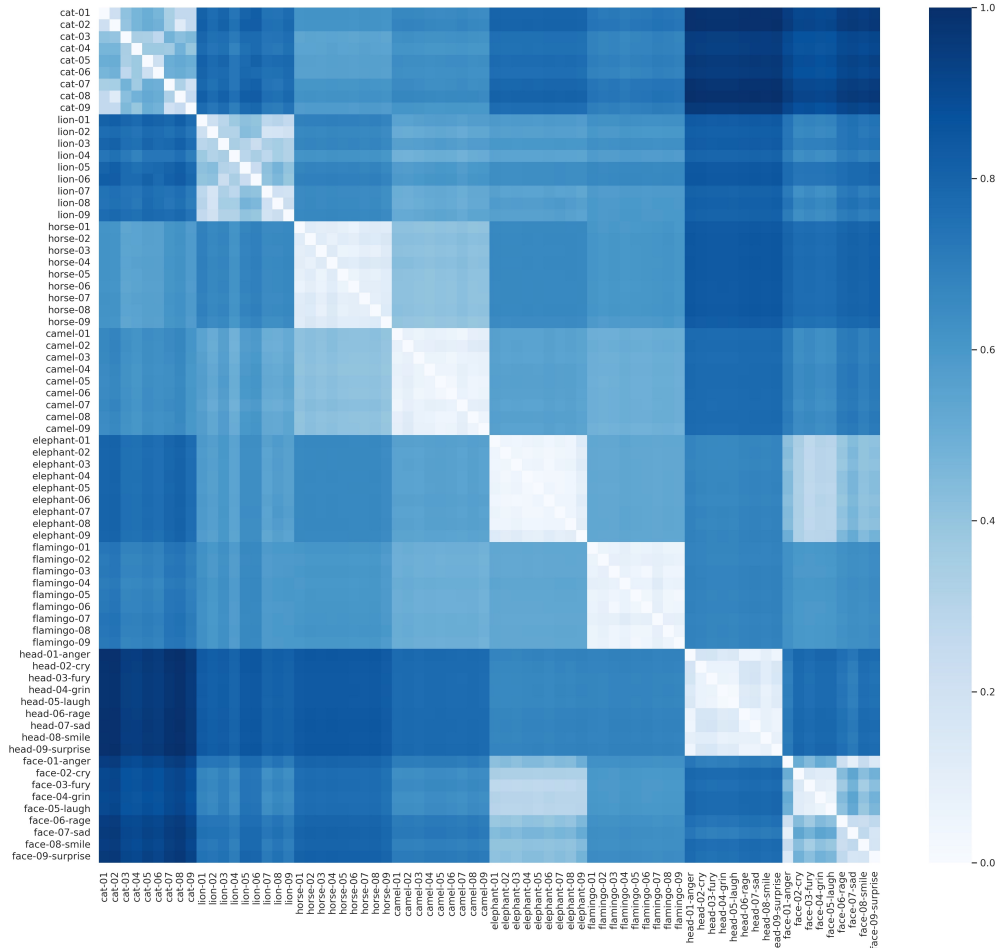


Figure 3: Distance matrix obtained for classification using GPS embeddings and  $G_2$  distribution.

constraints its usage in many cases.

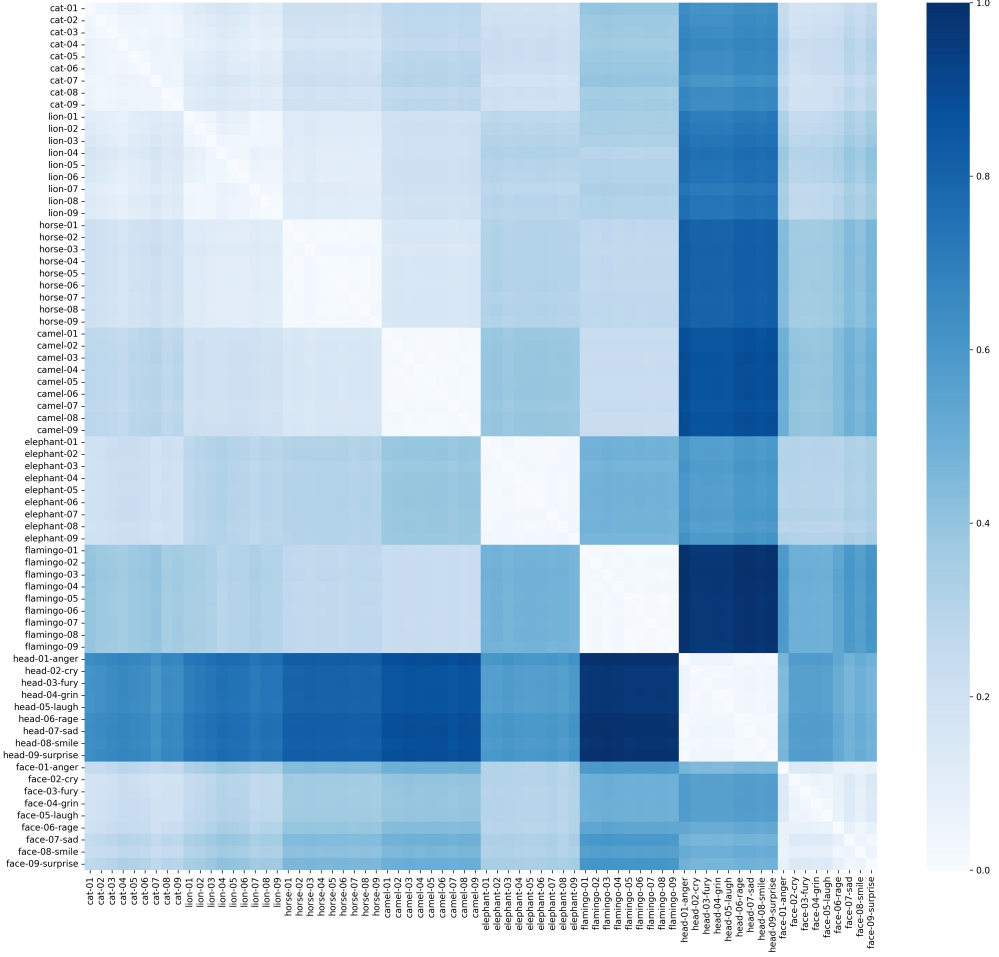


Figure 4: Distance matrix obtained for classification using Shape DNA embeddings.

## 7 Appendix

Laplace-Beltrami eigenvalues can be calculated for different object representations in different dimensions and for grayscale or color images. We consider a gray scale image as a surface defined by the graph of a height function being the gray scale intensity function of the image. The color image can, e.g. be understood as a surface (two-manifold) in a five-dimensional Euclidean space whose coordinates include the intensity parameters of the red, green, blue values assigned to any  $(x, y)$  pixel of the image. The Laplace-Beltrami operator can be applied to higher dimensions and also solids containing cavities for example, an ice-cube containing fully enclosed bubbles.

The spectra of Laplace-Beltrami does not meet the condition of [completeness](#) and so the name "fingerprint" might be misleading; instead, we use shape DNA to refer to this set of eigenvalues. Remember how two human twins have the same DNA but their fingerprints differ from each other. This spectra however satisfies other important characteristics that a fingerprint must meet: isometry, scaling, similarity, efficiency, etc. Here we introduce a different representation of Laplace-Beltrami operator that will be used later:

Let  $f$  be a real-valued function, with  $f \in C^2$ , defined on a Riemannian manifold  $M$ . Given a local parametrization as  $\psi : \mathbb{R}^n \rightarrow \mathbb{R}^{n+k}$  of a submanifold  $M$  of  $\mathbb{R}^{n+k}$ . The metric tensor  $g$  is

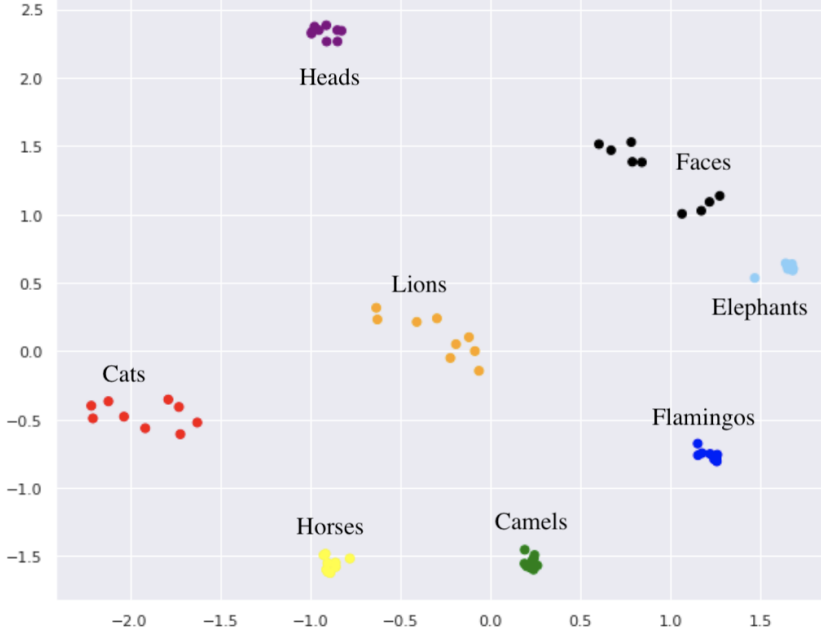


Figure 5: The Multidimensional scaling (MDS) of shape similarities computed using the  $G2$ -distributions. The dimension of the GPS embedding is  $d = 15$ ; the number of shells used is  $m = 8$ , which generates 36 histograms. The sum of  $L_2$  distances between respective histograms is used to compare two objects.

defined as:

$$g_{ij} := \langle \partial_i \psi, \partial_j \psi \rangle. \quad (10)$$

In the following we consider  $W$  to be the determinant of this tensor and  $g^{ij}$ 's the components of the inverse of the metric tensor. This way, we have the following formula for the Laplace-Beltrami operator applied to the function  $f$ :

$$\Delta f = \sum_{ij} \partial_i (g^{ij} W \partial_j f). \quad (11)$$

We have the following properties for the Laplace-Beltrami operator and its eigenvalues:

1. Spectrum is isometric invariant because the gradient and divergence only depend on the Riemannian structure of the manifold.
2. To compare manifolds in different scales we can normalize the eigenvalues. The scaled manifold has a parametrization as  $\bar{\psi} = a\psi$ . This implies  $\bar{W} = a^2 W$  and  $\bar{g}^{ij} = \frac{1}{a^2} g^{ij}$ . We can conclude that if  $u$  is a solution to  $\Delta_f u = -\lambda u$ , then  $u$  is also a solution to  $\Delta_{\bar{f}} u = -\frac{1}{a^2} \lambda u$ . This implies that scaling does not change the normalized set of eigenvalues.
3. For any finite sequence  $S = \{a_1 = 0 \leq a_2 \leq \dots \leq a_n\}$  there always exists a compact Riemannian manifold  $X$  with  $3 \leq \dim(X)$  with  $S$  as the beginning of its Laplace spectrum.
4. The spectrum cannot be compressed into a finite subsequence as a result of [mutual independence of eigenvalues](#).

5. We can however obtain a substantial amount of geometrical and topological just from the first few eigenvalues (approx. 500).
6. The spectrum does not completely determine the shape of the underlying manifold (Figure 6). In other words, we have distinct manifolds with the same spectra; however, there is some hope that isospectrality of non-isometric manifolds, at least in lower dimensions up to 3, is a relatively rare phenomenon. For instance, for the special case of surfaces with constant negative curvature, we have an upper bound for the number of isospectral but non-isometric surfaces depending only on the genus [Buser \[2010\]](#). For all of these reasons and also based on experimental studies, the spectra of the Laplace–Beltrami operator have significant discrimination power.

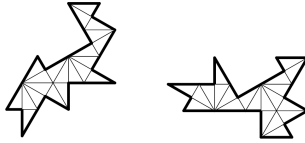


Figure 6: Isospectral domains

One theorem that can help to illustrate the point 5 is the following:

**Theorem 1 (Weyl—Asymptotic growth of eigenvalues)** *If  $D$  is a bounded region of  $\mathbb{R}^d$  with piecewise smooth boundary  $B$  and if  $0 \leq \lambda_1 \leq \lambda_2 \leq \dots$  is the spectrum and  $N(\lambda)$  the number of eigenvalues  $\leq \lambda$  counted with multiplicity, then:*

$$N(\lambda) \sim \frac{\omega_d \text{vol}(D) \lambda^{d/2}}{(2\pi)^d} \quad (12)$$

This theorem gives us a hint on how spectrum gives us geometric information and more accurate and precise derivations can be made from this point to further prove the importance of the eigenvalues of Laplace-Beltrami operator.

## 8 Definitions

### Congruence

Two geometric objects are congruent if they can be transformed into each other by rigid motions (translations and rotations) as well as reflections.

### Completeness

When a fingerprint gives a complete characterization of the shape it is considered to be complete.

### mutual independency of eigenvalues

An arbitrary eigenvalue  $\lambda_k$  of a compact Riemannian manifold cannot be computed from a finite number of other eigenvalues of when the manifold is unknown.

## References

Martin Reuter, Franz-Erich Wolter, and Niklas Peinecke. Laplace–beltrami spectra as ‘shape-dna’of surfaces and solids. *Computer-Aided Design*, 38(4):342–366, 2006.

- Raif M Rustamov. Laplace-beltrami eigenfunctions for deformation invariant shape representation. In *Proceedings of the fifth Eurographics symposium on Geometry processing*, pages 225–233, 2007.
- Robert W Sumner and Jovan Popovic. Mesh data from deformation transfer for triangle meshes, 2013.
- Herbert Seifert and William Threlfall. A textbook of topology. 1980.
- MP Do Carmo. Differential geometry of curves and surfaces (englewood cliff, nj, 1976.
- Ruben Wiersma, Elmar Eisemann, and Klaus Hildebrandt. Cnns on surfaces using rotation-equivariant features. *ACM Transactions on Graphics (TOG)*, 39(4):92–1, 2020.
- Rana Hanocka, Amir Hertz, Noa Fish, Raja Giryes, Shachar Fleishman, and Daniel Cohen-Or. Meshcnn: a network with an edge. *ACM Transactions on Graphics (TOG)*, 38(4):1–12, 2019.
- Lasse Hansen, Jasper Diesel, and Mattias P Heinrich. Multi-kernel diffusion cnns for graph-based learning on point clouds. In *Proceedings of the European Conference on Computer Vision (ECCV) Workshops*, pages 0–0, 2018.
- Nicholas Sharp, Souhaib Attaiki, Keenan Crane, and Maks Ovsjanikov. Diffusion is all you need for learning on surfaces. *arXiv preprint arXiv:2012.00888*, 2020.
- Bruno Vallet and Bruno Lévy. Spectral geometry processing with manifold harmonics. In *Computer Graphics Forum*, volume 27, pages 251–260. Wiley Online Library, 2008.
- Michael M Bronstein, Joan Bruna, Yann LeCun, Arthur Szlam, and Pierre Vandergheynst. Geometric deep learning: going beyond euclidean data. *IEEE Signal Processing Magazine*, 34(4):18–42, 2017.
- Peter Buser. *Geometry and spectra of compact Riemann surfaces*. Springer Science & Business Media, 2010.